Exploring the boundary of 3D perovskites domain: The case of $FAPb_{1-x}Sn_xBr_3$ perovskites

Ambra Pisanu,[a] Arup Mahata,[b,c] Edoardo Mosconi,[b,] Maddalena Patrini,[d] Paolo Quadrelli,[a] Chiara Milanese,[a] Filippo De Angelis,[b,c,*] Lorenzo Malavasi [a,*]*

[a]Department of Chemistry and INSTM, Viale Taramelli 16, Pavia, 27100 (Italy);

[b]Computational Laboratory for Hybrid/Organic Photovoltaics (CLHYO), CNR-ISTM, via Elce di Sotto 8, I-06123 Perugia, Italy

[c] D3-CompuNet, Istituto Italiano di Tecnologia, Via Morego 30, 16163 Genova, Italy

[d] Department of Physics and CNISM, Via Bassi 6, Pavia, 27100 (Italy)

Supporting Information

Experimental Section.

Samples of general formula $FAPb_{1-x}Sn_xBr_3$ (with nominal x=0, 0.05, 0.15, 0.3, 0.4, 0.6, 0.9, 1) were synthesized according to a general and original procedure we developed.[1-2] In a typical synthesis, a proper stoichiometric amount of Pb acetate and Sn acetate are dissolved in an HBr excess under continuous mechanical stirring under nitrogen atmosphere. Hypophosphoric acid is added to the solution and inert atmosphere is maintained in the reaction environment in order to prevent Sn oxidation. Then, the solution is heated to 100°C and the corresponding FA acetate solution (40%wt in water) is added in the stoichiometric amount. The solution is then cooled down to 46°C at 1°C/min, until the formation of a precipitate, which is immediately filtered and dried under vacuum overnight. Finally, the samples are treated at 100°C for 2 h before the characterization. The final products are handled and stored in a glove box with oxygen and water contents lower than 1 ppm.

All the reagents were purchased from Sigma Aldrich in pure form and were used without any further purification. The crystal structure of the samples has been characterized by room temperature Cu-radiation X-ray Powder Diffraction (XRD) in a Bruker D8 diffractometer by using a Bruker dome sealed in the glove box avoiding air exposure. The optical diffuse reflectance spectra of the different perovskites were measured from 0.8 to 4.5 eV (250-1500 nm, with step of 1 nm) by a Varian Cary 6000i equipped with an integrating sphere. For this kind of measurements polycrystalline powders were compacted into pellets of about 5 mm in diameter and reflectance spectra were calibrated using a standard reference disk. The real elemental composition of the samples was determined by Energy-dispersive X-ray spectroscopy using an INCA Energy 350 X Max detector from Oxford Instruments linked to the SEM. Cobalt standard was used for the calibration of the quantitative elementary analysis. All the samples manipulations were carried out under inert atmosphere thanks to a homemade sample holder allowing the transport of the powders from the glove box to the SEM chamber. Those analyses are essential to correlate the physical properties with the real stoichiometry instead of nominal cations ratio.

Computational Details

First-principles calculations based on density functional theory (DFT) are carried out as implemented in the PWSCF Quantum-Espresso package.[3] For geometry optimization, electrons-ions interactions were described by ultrasoft pseudo-potentials with electrons from I 5s, 5p; Br 4s, 4p; N, C 2s, 2p; H 1s; Pb, 6s, 6p, 5d; Sn 5s, 5p, 4d; Cs 5s, 5p, 6s; shells explicitly included in calculations.

Electronic structure are calculated by a single point hybrid calculations including SOC using the modified version of the HSE06 functional[4] including 43% Hartree-Fock exchange proposed in Ref.[5] with norm-conserving pseudo potentials with electrons from Br 4s, 4p; N, C 2s, 2p; H 1s; Pb 5s, 5p, 6s, 6p, 5d; Sn 4s, 4p, 5s, 5p, 4d; Cs 5s, 5p, 6s; shells explicitly included in calculations.

Single AMX_3 unit simulation

Geometry optimizations are performed with a k-point sampling[6] of 4x4x4 when using experimental cell parameters along with plane-wave basis set cutoffs for the smooth part of the wave functions and augmented electronic density expansions of 25 and 200Ry, respectively.

Variable cell optimization are performed a k-point sampling[6] of 8x8x8 including dispersion interaction[7] along with plane-wave basis set cutoffs for the smooth part of the wave functions and augmented electronic density expansions of 50 and 400Ry, respectively.

2x2x2 AMX_3 supercell simulation

Geometry optimizations are performed with a k-point sampling[6] of 2x2x2 when using experimental cell parameters along with plane-wave basis set cutoffs for the smooth part of the wave functions and augmented electronic density expansions of 25 and 200Ry, respectively.

HSE06-SOC calculation have been performed at Γ point with plane-wave basis set cutoffs for the smooth part of the wave functions and augmented electronic density expansions of 40 and 80Ry, respectively.

Isolated 0D $FASnBr_3$ model

We selected the optimized structure from the single $FASnBr_3$ unit calculation and we carried out a HSE06-SOC single point calculation with a large cell parameters (a=b=c=18.0 Å) at Γ point with plane-wave basis set cutoffs for the smooth part of the wave functions and augmented electronic density expansions of 40 and 80Ry, respectively.

3x3x3 $FASnBr_3$ molecular dynamic simulation

Car-Parrinello Molecular Dynamics[8-9] have been carried out using a 3x3x3 supercell $FASnBr_3$ model generated by duplicating the 1x1x1 optimized structure using the experimental cell parameters. Electrons-ions interactions were described by ultrasoft pseudo-potentials with electrons

from Br 4s, 4p; N, C 2s, 2p; H 1s; Sn 5s, 5p, 4d; shells explicitly included in calculations. Plane-wave basis set cutoffs for the smooth part of the wave functions and augmented electronic density expansions of 25 and 200Ry, respectively. A time step of 10 a. u., electronic mass of 1000 a.u. and masses equal to 5.0 a.m.u have been used for all atoms. The simulation has been carried out at 319 K for a simulation time of 14 ps comprising the initial thermalization.

On selected snapshots from 4 to 6 ps, we carried out a single point calculation with ultra-soft pseudo potential at PBE-GGA level of theory with plane-wave basis set cutoffs for the smooth part of the wave functions and augmented electronic density expansions of 25 and 200Ry, respectively. The results are reported in Figure S3.

"Short/Long" inversion reaction pathway

For the $FASnBr_3$ and $FAGeI_3$ with simulate the reaction energy profile of the inversion of one short/long M-X bond to evaluate the reaction barriers. We simulate the 1x1x1 unitary $FASnBr_3$ and $FAGeI_3$ using fixed experimental cell parameter, 4x4x4 k-point sampling, PBE ultra-soft pseudo potentials, with plane-wave basis set cutoffs for the smooth part of the wave functions and augmented electronic density expansions of 25 and 200Ry, respectively.

Table S1. Relaxed cell parameters (Å) of the 1x1x1 pseudo-cubic $FAPbBr_3$ and $FASnBr_3$ structures.

	a	b	c	Exp.
$FAPbBr_3$	5.989	6.011	5.964	5.995
$FASnBr_3$	5.930	6.140	5.883	6.034

Table S2. Relative stabilities and calculated band-gap of the $FAPb_{0.5}Sn_{0.5}Br_3$ with different Sn and Pb positions. Geometries reported in Figure S1.

	E (eV)	GAP (PBE-GGA)	GAP (HSE-SOC)
1	0.00	1.52	1.94
2	0.11	1.42	-
3	0.09	1.58	-

4	0.14	1.50	-
5	0.17	1.47	-

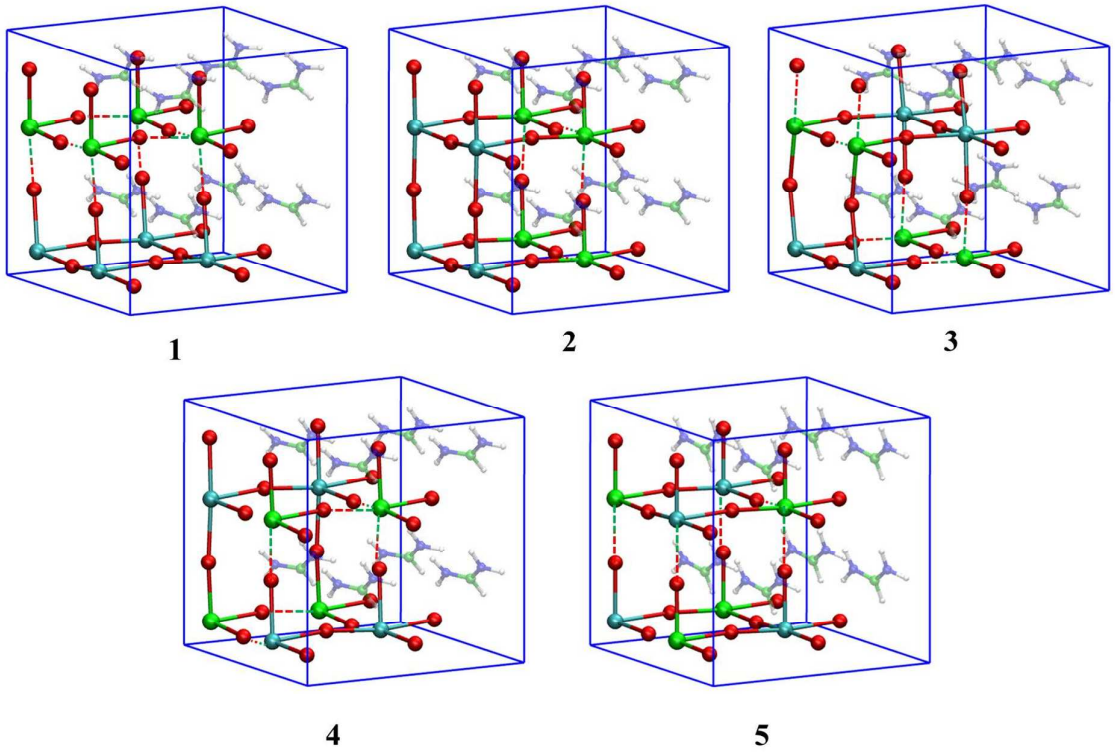

Figure S1. $FAPb_{0.5}Sn_{0.5}Br_3$ cubic possible Sn and Pb positions. Light blue: Pb; Green: Sn; Red: Br. FA cations are shaded in the background for clarity.

Table S3. Calculated short-long metal-halide bond lengths (Å) and experimental band-gaps (E_g, eV) for a series of cubic perovskites varying A, M and X. Band-gaps are taken from the corresponding references. Calculated data are compared to experimental data for $AGeI_3$ perovskites.[10]

A	M	X	[100]	[010]	[001]	Avg.	E_g
FA	Sn	Br	2.81, 3.24	2.76, 3.30	2.80, 3.24	2.79, 3.26	2.37
MA	Sn	Br	2.81, 3.09	2.83, 3.08	2.83, 3.08	2.82, 3.08	2.00[a]
Cs	Sn	Br	2.88, 2.92	2.87, 2.93	2.87, 2.93	2.87, 2.93	1.75[b]
FA	Sn	I	3.09, 3.18	3.02, 3.28	3.09, 3.18	3.07, 3.21	1.41[c]
MA	Sn	I	3.03, 3.20	3.02, 3.23	3.02, 3.23	3.02, 3.22	1.20[c]
Cs	Sn	I	3.07, 3.13	3.06, 3.14	3.06, 3.14	3.06, 3.14	1.27[d]
FA	Pb	Br	3.00, 3.00	3.02, 3.03	2.98, 3.02	3.00, 3.02	2.18
MA	Pb	Br	2.94, 2.99	2.93, 3.02	2.92, 3.02	2.93, 3.01	2.20[e]
FA	Pb	I	3.16, 3.24	3.19, 3.27	3.19, 3.25	3.18, 3.25	1.48[c*]
MA	Pb	I	3.16, 3.18	3.10, 3.25	3.10, 3.25	3.12, 3.23	1.52[c]

FA	Ge	I	-	-	-	2.75, 3.26	2.2[f]
MA	Ge	I	-	-	-	2.77, 3.45	1.9[f]
Cs	Ge	I	-	-	-	2.73, 3.58	1.6[f]

[a] Ref. [11]; [b] Ref. [12]; [c] Ref. [13]; [d] Ref. [14]; [e] Ref. [1]; [f] Ref. [10]
* This result are referred to the P3m1 structure as reported in Ref. [13]

Table S4. Cell parameters used for geometry relaxations of AMX_3.

A	M	X	a	b	c	References
FA	Sn	Br	12.068	12.068	12.068	This paper
MA	Sn	Br	11.816	11.816	11.816	[a] Ref. [11]
Cs	Sn	Br	5.798	5.798	5.798	[b] Ref. [12]
FA	Sn	I	12.512	12.517	12.517	[c] Ref. [13]
MA	Sn	I	6.230	6.230	6.232	[c] Ref. [13]
Cs	Sn	I	6.199	6.199	6.199	[d] Ref. [14]
FA	Pb	Br	11.991	11.991	11.991	This paper
MA	Pb	Br	11.861	11.861	11.861	[e] Ref. [1]
FA	Pb	I	8.982	8.982	11.01	[c] Ref. [13]*
MA	Pb	I	6.312	6.312	6.315	[c] Ref. [13]

* This are referred to the P3m1 structure from Ref. [13]

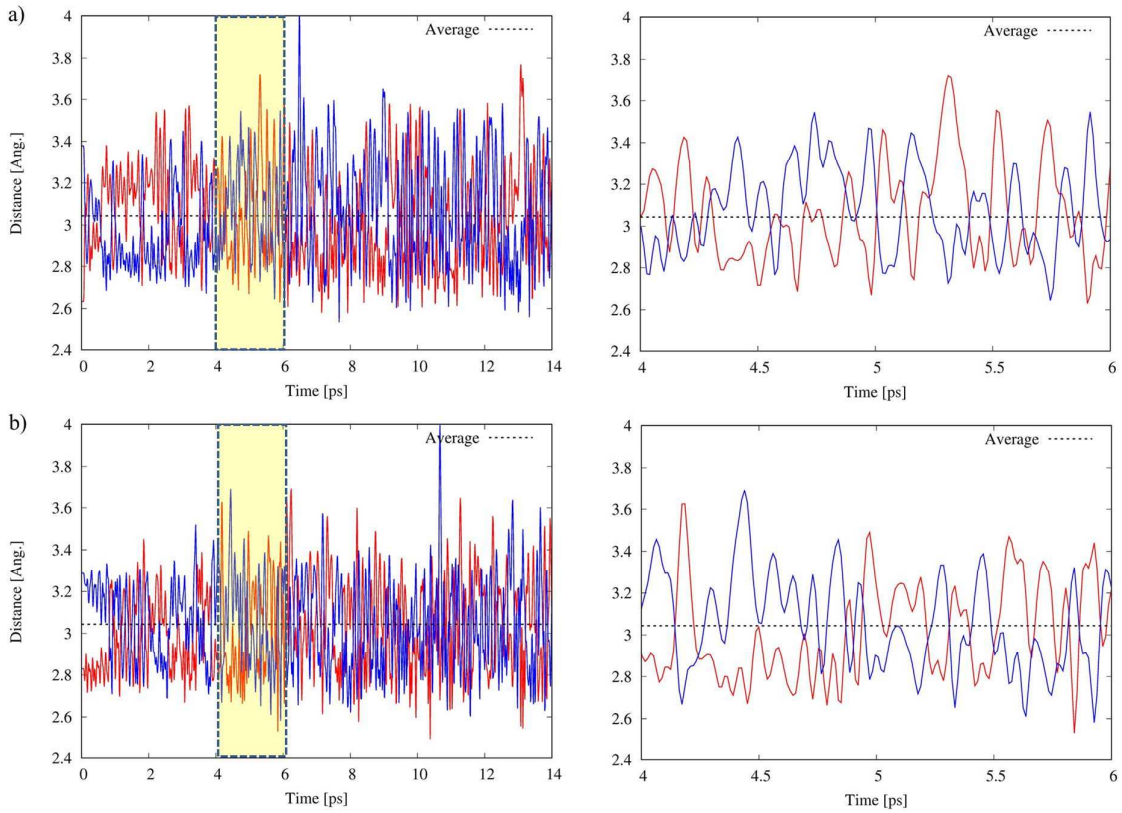

Figure S2. Time evolution of Sn-Br bond distances for a selected Sn center along (a) [100] and (b) [010] direction. The panels on the right show a detail of the time from 4 to 6 ps highlighted by the yellow rectangle on the left panels. Red (blue) lines refer to initially short (long) Sn-Br distances.

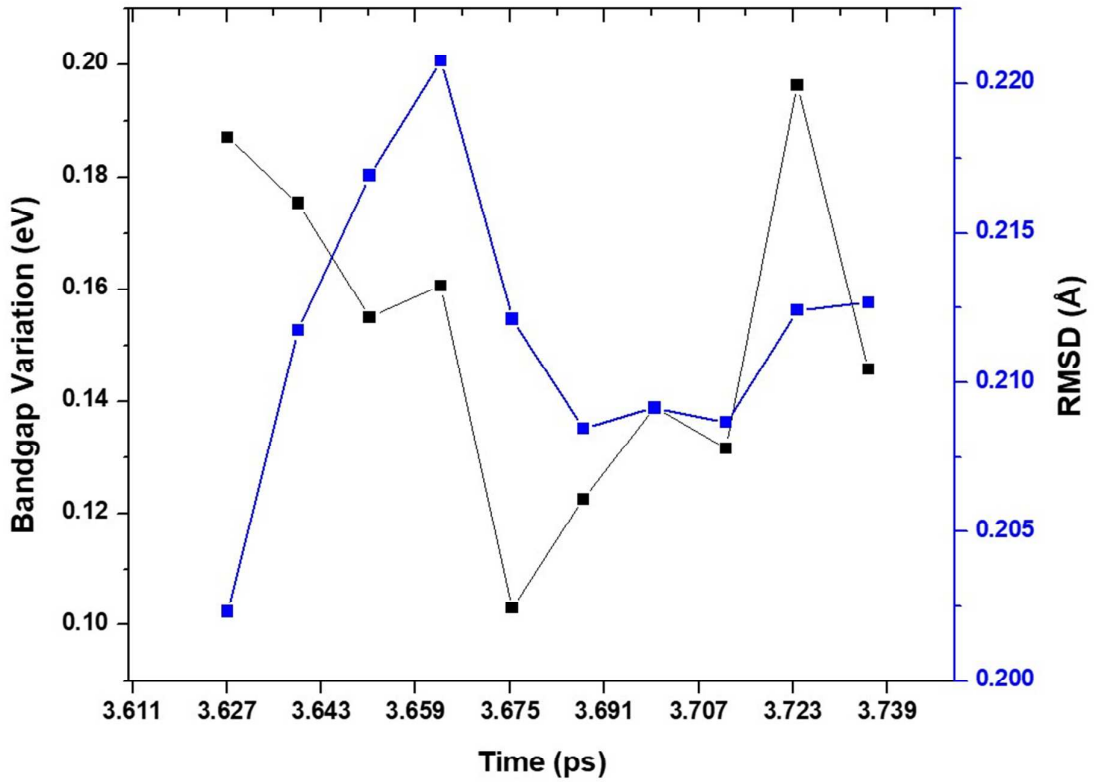

Figure S3. Variation of bandgap at different time of the simulation with the corresponding RMSD value. The band gap variation has been plotted with respect to the optimized 3x3x3 cubic supercell of $FASnBr_3$ at GGA-PBE level of theory. The band gap variation is referred to the band gap of the optimized system (1.36 eV) calculated at the same level of theory.

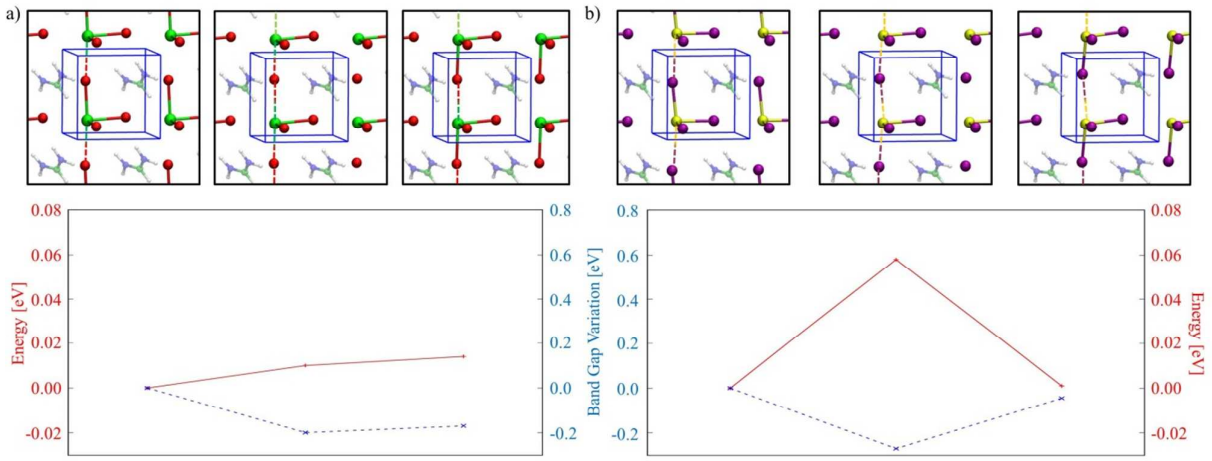

Figure S4. Energy and band gap variation profile of the M-X bond from "short" to "long" configuration for $FASnBr_3$ (a) and $FAGeI_3$ (b).

References:

(1) Mancini, A.; Quadrelli, P.; Milanese, C.; Patrini, M.; Guizzetti, G.; Malavasi, L. CH3NH3SnxPb1–xBr3 Hybrid Perovskite Solid Solution: Synthesis, Structure, and Optical Properties. *Inorg. Chem.* **2015**, *54*, 8893-8895.
(2) Mancini, A.; Quadrelli, P.; Amoroso, G.; Milanese, C.; Boiocchi, M.; Sironi, A.; Patrini, M.; Guizzetti, G.; Malavasi, L. Synthesis, structural and optical characterization of APbX3 (A=methylammonium, dimethylammonium, trimethylammonium; X=I, Br, Cl) hybrid organic-inorganic materials. *J. Solid State Chem.* **2016**, *240*, 55-60.
(3) Giannozzi, P.; Baroni, S.; Bonini, N.; Calandra, M.; Car, R.; Cavazzoni, C.; Ceresoli, D.; Chiarotti, G. L.; Cococcioni, M.; Dabo, I., et al. QUANTUM ESPRESSO: A Modular and Open-Source Software Project for Quantum Simulations of Materials. *J. Phys.: Condens. Matter* **2009**, *21*, 395502.
(4) Heyd, J.; Scuseria, G. E.; Ernzerhof, M. Hybrid functionals based on a screened Coulomb potential. *J. Chem. Phys.* **2003**, *118*, 8207-8215.
(5) Du, M.-H. Density Functional Calculations of Native Defects in CH3NH3PbI3: Effects of Spin–Orbit Coupling and Self-Interaction Error. *J. Phys. Chem. Lett.* **2015**, *6*, 1461-1466.
(6) Monkhorst, H. J.; Pack, J. D. Special points for Brillouin-zone integrations. *Phys. Rev. B* **1976**, *13*, 5188-5192.
(7) Grimme, S.; Antony, J.; Ehrlich, S.; Krieg, H. A consistent and accurate ab initio parametrization of density functional dispersion correction (DFT-D) for the 94 elements H-Pu. *J. Chem. Phys.* **2010**, *132*, 154104.
(8) Car, R.; Parrinello, M. Unified Approach for Molecular Dynamics and Density-Functional Theory. *Phys. Rev. Lett.* **1985**, *55*, 2471-2474

(9) Giannozzi, P.; Angelis, F. D.; Car, R. First-principle molecular dynamics with ultrasoft pseudopotentials: Parallel implementation and application to extended bioinorganic systems. *J. Chem. Phys.* **2004**, *120*, 5903-5915.
(10) Stoumpos, C. C.; Frazer, L.; Clark, D. J.; Kim, Y. S.; Rhim, S. H.; Freeman, A. J.; Ketterson, J. B.; Jang, J. I.; Kanatzidis, M. G. Hybrid Germanium Iodide Perovskite Semiconductors: Active Lone Pairs, Structural Distortions, Direct and Indirect Energy Gaps, and Strong Nonlinear Optical Properties. *J. Am. Chem. Soc.* **2015**, *137*, 6804-6819.
(11) Ferrara, C.; Patrini, M.; Pisanu, A.; Quadrelli, P.; Milanese, C.; Tealdi, C.; Malavasi, L. Wide band-gap tuning in Sn-based hybrid perovskites through cation replacement: the FA1-xMAxSnBr3 mixed system. *J. Mater. Chem. A* **2017**, *5*, 9391-9395.
(12) Gupta, S.; Bendikov, T.; Hodes, G.; Cahen, D. CsSnBr3, A Lead-Free Halide Perovskite for Long-Term Solar Cell Application: Insights on SnF2 Addition. *ACS Energy Lett.* **2016**, *1*, 1028-1033.
(13) Stoumpos, C. C.; Malliakas, C. D.; Kanatzidis, M. G. Semiconducting Tin and Lead Iodide Perovskites with Organic Cations: Phase Transitions, High Mobilities, and Near-Infrared Photoluminescent Properties. *Inorg. Chem.* **2013**, *52*, 9019-9038.
(14) Sabba, D.; Mulmudi, H. K.; Prabhakar, R. R.; Krishnamoorthy, T.; Baikie, T.; Boix, P. P.; Mhaisalkar, S.; Mathews, N. Impact of Anionic Br– Substitution on Open Circuit Voltage in Lead Free Perovskite (CsSnI3-xBrx) Solar Cells. *J. Phys. Chem. C* **2015**, *119*, 1763-1767.